AGU PUBLICATIONS

JGR

Journal of Geophysical Research: Planets

REVIEW ARTICLE

10.1002/2016JE005119

Special Section:
JGR-Planets 25th Anniversary

Key Points:
- Cometary surfaces include a diverse range of landforms reflecting the variety of processes that formed them
- Among the key mechanisms active on cometary surfaces are sublimation, sedimentary processes, and fracturing
- All morphologies do not exist on all comets and certain landforms (e.g., flows and spires) are unique to specific nuclei

Correspondence to:
J. M. Sunshine,
jess@astro.umd.edu

Citation:
Sunshine, J. M., N. Thomas, M. R. El-Maarry, and T. L. Farnham (2016), Evidence for geologic processes on comets, *J. Geophys. Res. Planets*, *121*, 2194–2210, doi:10.1002/2016JE005119.

Received 23 JUN 2016
Accepted 20 SEP 2016
Published online 7 NOV 2016

©2016. American Geophysical Union. All Rights Reserved.

source: https://doi.org/10.7892/boris.113772 | downloaded: 12.10.2024

Evidence for geologic processes on comets

Jessica M. Sunshine[1], Nicolas Thomas[2], Mohamed Ramy El-Maarry[2], and Tony L. Farnham[1]

[1]Department of Astronomy, University of Maryland, College Park, Maryland, USA, [2]Physikalisches Institut, University of Bern, Bern, Switzerland

Abstract Spacecraft missions have resolved the nuclei of six periodic comets and revealed a set of geologically intriguing and active small bodies. The shapes of these cometary nuclei are dominantly bilobate reflecting their formation from smaller cometesimals. Cometary surfaces include a diverse set of morphologies formed from a variety of mechanisms. Sublimation of ices, driven by the variable insolation over the time since each nucleus was perturbed into the inner Solar System, is a major process on comets and is likely responsible for quasi-circular depressions and ubiquitous layering. Sublimation from near-vertical walls is also seen to lead to undercutting and mass wasting. Fracturing has only been resolved on one comet but likely exists on all comets. There is also evidence for mass redistribution, where material lifted off the nucleus by subliming gases is deposited onto other surfaces. It is surprising that such sedimentary processes are significant in the microgravity environment of comets. There are many enigmatic features on cometary surfaces including tall spires, kilometer-scale flows, and various forms of depressions and pits. Furthermore, even after accounting for the differences in resolution and coverage, significant diversity in landforms among cometary surfaces clearly exists. Yet why certain landforms occur on some comets and not on others remains poorly understood. The exploration and understanding of geologic processes on comets is only beginning. These fascinating bodies will continue to provide a unique laboratory for examining common geologic processes under the uncommon conditions of very high porosity, very low strength, small particle sizes, and near-zero gravity.

1. Introduction

Comets are among the most spectacular objects in the night sky. Moreover, they contain the most accessible record of the primitive ices and dust that coalesced in the protosolar nebula. Yet until relatively recently, their nuclei have either been shrouded by activity from subliming gases when in the inner Solar System or remained hidden due to their inherent dark albedo (~4%) when far from the Sun and inactive. In the era of international spacecraft exploration to periodic comets, during which cometary nuclei have been imaged with increasing resolution, comets have expanded from rich targets for astronomical study to the geologically intriguing objects that we now know to be a diverse group of small worlds.

In 1986, ESA's Giotto [*Keller et al*., 1986] and the Soviet Vega 1 and 2 [*Sagdeev et al*., 1986] missions to 1P/Halley ($16 \times 8 \times 8$ km) provided the first resolved images of a cometary nucleus. Even at maximum resolution of ~50 m/pix with challenging lighting conditions, the nucleus of Halley showed an unexpectedly complex morphology with discernable surface features [e.g., *Basilevsky and Keller*, 2006]. It would be another 15 years before the next cometary flyby, NASA's Deep Space 1 technology demonstration at 19P/Borrelly ($8 \times 4 \times 4$ km), which had a maximum resolution of 43 m/pix and revealed an elongated and bent nucleus that for the first time included distinct morphologic units [*Soderblom et al*., 2002]. NASA's Discovery Program included three subsequent cometary missions, which acquired images from four flybys of three additional comets. In 2004, Stardust, a coma sample return mission, imaged 81P/Wild 2 ($5.5 \times 4.0 \times 3.3$ km) with a maximum resolution of 14 m/pix revealing a nucleus covered in various depressions [*Brownlee et al*., 2004]. Deep Impact's mission to 9P/Tempel 1 (oblong, with diameters from 5 to 7.5 km) [*Thomas et al*., 2013a] in 2005 was the first planetary-scale impact experiment and observed a geologically complex nucleus including multiple kilometer-scale smooth flows at resolutions up to 7.3 m/pix [*A'Hearn et al*., 2005; *Thomas et al*., 2007]. After the Tempel 1 impact event, the surviving Deep Impact flyby spacecraft was used for an extended mission. The Deep Impact Extended Investigation (DIXI) to 103P/Hartley 2 ($0.7 \times 0.7 \times 2.3$ km) [*Thomas et al*., 2013b] in 2010 observed a small, very active comet with resolutions up to 6.9 m/pix [*A'Hearn et al*., 2011]. For its extended mission in 2011, the Stardust spacecraft returned to Tempel 1 (Stardust New Exploration of Tempel-NExT) and, in comparison to images from the Deep Impact encounter, revealed changes on a cometary nucleus including retreat of the large flow [*Veverka et al*., 2013]. The collection of images acquired

with these flyby missions provides a basis for comparison to the ongoing ESA mission to 67P/Churyumov-Gerasimenko (C-G). Unlike previous flybys, Rosetta is a well-instrumented mission that includes both an orbiter and a lander (Philae) and orbits with the comet from ±3.5 AU including through the comet's perihelion. With centimeter-scale orbital imagery and millimeter-scale images from the lander, Rosetta's extensive temporal and spatial coverage of C-G provides by far the best resolution data for any cometary nucleus.

These missions have revealed a set of cometary nuclei that are morphologically complex and among the most geologically active objects in the Solar System. Comparisons, even among this limited set of objects, have also allowed us to recognize common landforms and processes as well as surprisingly distinct differences. Furthermore, the unique characteristics of comets, with their very low density (~0.5 g/cm^3), high porosity (>75% voids), near-zero inferred strength, fine particles, and microgravity environment, provide unusual regimes for examining geologic processes. At global scales, the surfaces of cometary nuclei reflect the primitive conditions of their formation, while individual landforms result from evolutionary processes that are largely driven by the accumulated effects of insolation. Over geologic timescales comets are inactive. However, once perturbed into the inner Solar System, they can change over tens to thousands of years as their constituent ices sublime, dragging dust grains off their surfaces. Even in the microgravity of a comet, some of these grains will return to the surface leading to sedimentary features not predicted for cometary surfaces. Fracturing is also now recognized as a major process on cometary surfaces. Additionally, given their low strength, even the small gravity of a comet has significant effects on its morphology.

While insolation is a major force on comets, it is highly variable. Globally, the effect of solar heating is a function of the length of time a comet has been in the inner Solar System and its current orbit, which typically ranges over several AU. In addition, insolation varies seasonally and diurnally, both of which are dependent on the comet's rotation and pole position. For example, C-G has extreme seasonal variations with the southen hemisphere in sunlight only for a few months around perihelion. Furthermore, the irregular bulk shape and local topography of a cometary nucleus can also significantly affect local insolation.

The assessment that follows is not intended to be comprehensive but instead highlights some of the interesting features seen on the surfaces of all cometary nuclei observed to date and the key geologic processes from which they result. This work builds directly on previous comparisons of geomorphology on comets, which revealed surprising diversity on what was expected to be geologically simple bodies [e.g., *Basilevsky and Keller*, 2006]. The wealth of recent data of cometary surfaces, acquired over the last decade with increasing spatial resolution, provides unambiguous evidence of geologic diversity on individual comets. These new data also facilitate comparisons among cometary surfaces that often point to common geological processes. Yet despite the disparity in resolution among images of comets, it is also clear that individual comets exhibit different, sometimes unique, geomorphologic features. Some geologic processes, for reasons largely not understood, are therefore either not active on all comets or manifest differently on some comets than on others. Thus, even the high-resolution images of C-G do not provide the best data set for understanding all geological features observed on comets. This review is a snapshot in time during the ongoing Rosetta mission at C-G, which most notably is before the highest resolution data collection prior to and during the final approach to the landing of the orbiter. Many exciting new insights will arise from analyses of these data and the continued integration of existing data from Rosetta with those from previous missions to other comets.

2. The Bulk Properties of Cometary Nuclei

Although comets were first described as "dirty snowballs" and later as "icy dirtballs," since the first comet nucleus was resolved from the Halley flybys [*Keller et al*., 1986; *Sagdeev et al*., 1986], we have known that their shapes are far from spherical. Of the six cometary nuclei resolved by spacecraft imaging (Figure 1) only one, Wild 2, can easily be characterized as an oblate spheroid [*Duxbury et al*., 2004]. At the other extreme, C-G clearly consists of two lobes [*Sierks et al*., 2015], and both Hartley 2 [*A'Hearn et al*., 2011] and Borrelly [*Soderblom et al*., 2002] each have distinct ends. While less obvious, the side of Tempel 1 observed by Deep Impact also consists of two topographic facets separated by a scarp several hundreds of meters high giving it an overall pyramidal shape [*Thomas et al*., 2007]. The bulk shapes of these five nuclei strongly suggest that they are formed from smaller bodies or cometesimals. The dominance (5 of 6) of bilobe versus singular or multilobe nuclei argues for a formation process that favors the creation of coequal-sized binary cometesimals, which may be possible under some current cometary formation models [e.g., *Jansson and Johansen*, 2014].

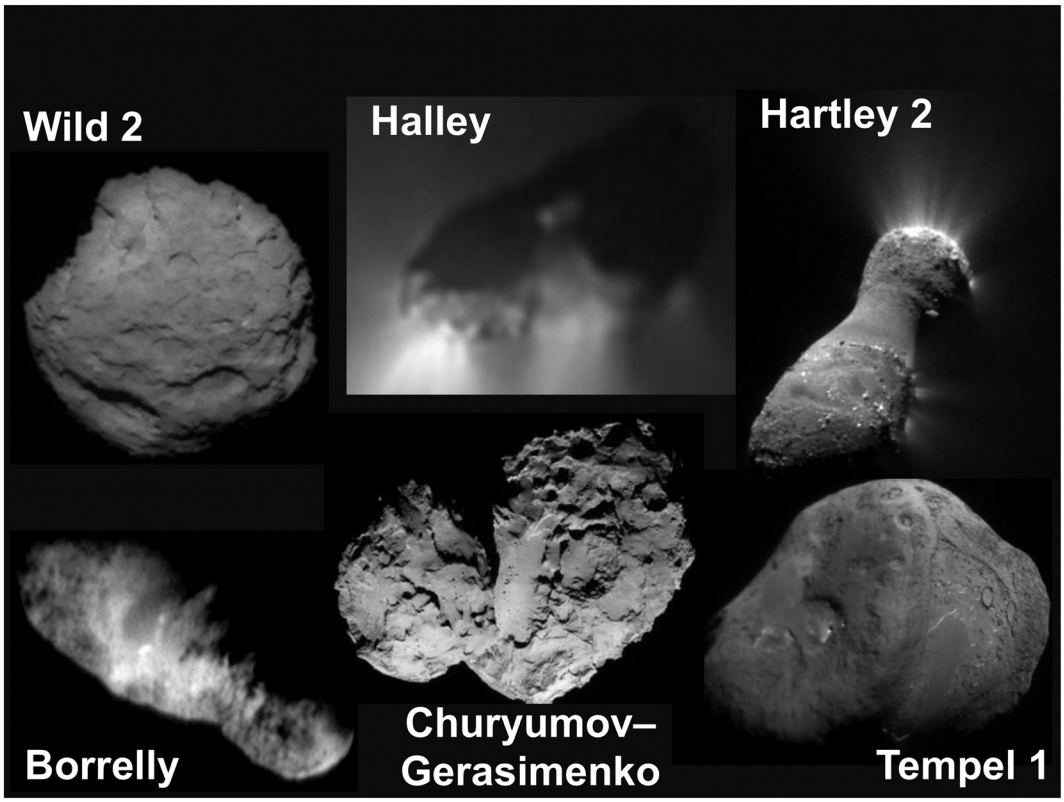

Figure 1. The ensemble of cometary nuclei that have been resolved by spacecraft imaging reveals a diversity of shapes and morphologic features. Except for Wild 2, all nuclei have bulk shapes that are bilobate, suggesting a common formation from smaller cometesimals. (Not to scale. See text for nuclei dimensions.)

In addition to maintaining cometesimals, cometary formation mechanisms must also allow for the very low density and bulk porosity that has been consistently inferred for the nuclei. For example, *Crawford* [1997] modeled the breakup of comet Shoemaker-Levy 9 and concluded that prior to breakup the comet had a density of 0.25 g/cm^3. *Farnham and Cochran* [2002] used orbital perturbations and observations of the jet's gas emission to derive a mass for Borrelly, which, when combined with the volume of Borrelly determined from Deep Space 1 images [*Soderblom et al*., 2002], led to an estimate of the bulk density of 0.49 g/cm^3. A major result of the Deep Impact experiment [*A'Hearn et al*., 2005] was the determination that Tempel 1 had a very high bulk porosity [*Schultz et al*., 2007; *Ernst and Schultz*, 2007] in the range of 50–88% [*Davidsson et al*., 2007] and a bulk density of 0.4–0.5 g/cm^3 [*Richardson et al*., 2007; *Holsapple and Housen*, 2007; *Davidsson et al*., 2007]. Inferring a high porosity is a consequence of the low bulk density. When combining ices with densities ~1 g/cm^3 and silicates with densities ~2.5 g/cm^3, a porosity of 50–90% is necessary to give the low density observed in comets. This very high porosity was confirmed by Rosetta gravity and shape measurements of C-G, which found a globally homogenous nucleus with density of 0.553 ± 0.006 g/cm^3 and a porosity of 72–74% [*Pätzold et al*., 2016]. Based on all of these studies, it is clear that low density and high porosity are fundamental properties of comets, and to preserve these characteristics, cometesimals must have accreted at very low velocities (~ m/s) [e.g., *Jutzi and Asphaug*, 2015].

Despite these morphologic indications for cometesimals, evidence for compositional heterogeneity on cometary nuclei remains limited to the detection of small patches of water ice [e.g., *Sunshine et al*., 2007a]. Only four cometary missions have collected color or near-infrared spectrometer data that could be used to investigate possible variations in surface composition. The first resolved observations of a cometary nucleus were Deep Space 1 spectra (1.3 to 2.5 μm) of Borrelly, which revealed a red sloped nucleus with a potential organic feature at 2.39 μm and only minor variations in slope along the nucleus [*Soderblom et al*., 2004]. However, these data were limited in spatial resolution (~160 m by the width of the comet) and by saturation [*Soderblom et al*., 2004]. Deep Impact's observations with an infrared spectrometer (1–5 μm) and two

multispectral imagers also found generally featureless red sloped nuclei from flybys of both Tempel 1 and Hartley 2 [*Li et al*., 2007, 2013]. However, for the first time, Deep Impact's infrared spectral data of Tempel 1, collected prior to the impact event, discovered small isolated patches of water ice on the surface of a comet that were also enhanced in blue and near-UV images [*Sunshine et al*., 2007a]. Similarly at Hartley 2, Deep Impact observations indicated that there were water ice-rich regions on the nucleus, but only along the morning terminator suggesting they may be frost deposits [*Sunshine et al*., 2011]. *Rubin et al*. [2014] demonstrated that this mechanism was plausible using a gas dynamics model. With the exception of slope, neither Tempel 1 nor Hartley 2 showed any variation in surface composition in either infrared spectra or multispectral images. In particular, there were no discernible compositional differences between the two ends of Hartley 2 or among any morphologic regions on Tempel 1. Although Rosetta has much higher spatial resolution and longer orbital coverage, the rendezvous with C-G yielded very similar compositional results: small variations in overall red spectral slopes [*Capaccioni et al*., 2015], discrete ice deposits seen both in color images [*Pommerol et al*., 2015; *Fornasier et al*., 2015] and visible near-infrared (0.2–5 μm) spectroscopy [*De Sanctis et al*., 2015], and a more or less uniform broad (2.9–3.6 μm) feature potentially related to organics [*Capaccioni et al*., 2015]. Like the other comets, C-G does not appear to have significant compositional variability across its surface, despite the presence of substantial morphologic diversity [*Thomas et al*., 2015a] and two distinct lobes.

This lack of variation in surface composition may reflect relatively uniform processing (e.g., lag deposits from sublimation of ices) in the thin uppermost layer accessible by spectroscopy. Typical surface temperatures within 1.5 AU from the Sun have been known to be higher than the free sublimation temperature of water ice since the measurements of Halley made by the thermal infrared spectrometer on Vega 1 [*Emerich et al*., 1987]. Subsequent more detailed measurements at Tempel 1 [*Groussin et al*., 2013] suggest thermal inertia values of $<50\,\mathrm{W/K/m^2/s^{1/2}}$. Although low, diurnal and seasonal thermal waves can still reach centimeters and decimeters, respectively [*Sunshine et al*., 2007b; *Thomas et al*., 2008]. Thus, differences in outgassing of subliming ice can probe potential heterogeneities from deeper in the interior. Variations in CO_2/H_2O across comet Tempel 1 from Deep Impact observations are suggestive of heterogeneities; however, from a flyby, diurnal and seasonal effects cannot be ruled out [*Feaga et al*., 2007]. Similar ambiguity exists in interpreting variability in volatiles from telescopic data that provide snapshots of a comet's orbit [*Mumma and Charnley*, 2011]. Even Rosetta, in orbit from ±3 AU has been unable to resolve compositional differences in outgassing from the two lobes of C-G because the comet is highly affected by seasons, which results in the Southern Hemisphere being only briefly in sunlight near perihelion [*Keller et al*., 2015]. Rosetta's effort to discern compositional heterogeneity related to cometesimals has been further complicated by the early demise of its primary volatile mapping capability when the cryocooler for the Visible and Infrared Thermal Imaging Spectrometer-Mapping (VIRTIS-M) infrared detector prematurely failed on 3 May 2015 at 2.5 AU, well before perihelion [*Fink et al*., 2016]. Strong variations in the CO_2/H_2O gas density ratio were observed by the Rosetta Orbiter Spectrometer for Ion and Neutral Analysis (ROSINA) mass spectrometer, but seasonal effects may be dominating these variations [*Hässig et al*., 2015].

The best example of compositional heterogeneity across a cometary nucleus comes from Hartley 2. Compared to Deep Impact observations at Tempel 1, spectral data of Hartley 2 have increased signal to noise due to both decreased heliocentric distance and a much more active comet. This facilitated the spectral monitoring of outgassing from farther distances and thus over several rotation cycles. In addition, Hartley 2 is in complex rotation [*Thomas et al*., 2013b], which over months provides near-uniform insolation, and thus no appreciable seasonal effects. Significant differences in CO_2/H_2O (~2 times) were detected between the two ends of Hartley 2 providing the first evidence that the cometesimals within a single comet are compositionally distinct [*A'Hearn et al*., 2011, 2012; *Feaga et al*., 2011]. Such internal compositional heterogeneity among cometesimals suggests mixing within the solar nebula at timescales between the initial growth of cometesimals and subsequent planetary migration [*A'Hearn et al*., 2012].

3. Fracturing

At smaller scales, the surfaces of cometary nuclei are heterogeneous. In some cases smooth terrains contrast sharply with rougher surfaces producing a rock-like appearance. In addition, many surfaces, especially those seen on C-G in the highest resolution data, show extensive fracturing. Fractures may develop on the surface

of a comet through thermal processing, which mainly operates on a diurnal scale, or from seasonal thermal contraction, which operates on a longer timescale. However, thermal insolation weathering can be a main agent in fracturing and eventual mechanical breakdown of surface materials on dry airless bodies [e.g., *Dombard et al*., 2010; *Delbo et al*., 2014; *Molaro et al*., 2015] and may even play a role in the formation of lineations on asteroids [*Dombard and Freed*, 2002]. Seasonal thermal contraction, however, generally occurs in ice-rich surface materials and requires lower thermal gradients and ranges than those required for thermal insolation weathering. This results in the formation of more organized fracture patterns (in response to the more homogenous and slowly evolving stress field) commonly observed in high latitudes on Earth and midlatitudes to high latitudes on Mars [e.g., *Levy et al*., 2010].

The airless nature of comets and their ice-rich composition should, in theory, facilitate the development of fractures as long as the surfaces are hard enough to sustain them, but earlier cometary missions were not able to offer unambiguous evidence of fractures mainly due to imaging resolution constraints. Instead, studies focused on modeling to infer conditions of fracture development and propagation [e.g., *Kührt*, 1984; *Tauber and Kührt*, 1987]. However, high-resolution ($<$20 cm/pixel) images from Rosetta have shown that most of the comet's surface is dominated by consolidated materials, which are indeed often fractured (Figure 2) [*Thomas et al*., 2015a; *El-Maarry et al*., 2015a]. The fractures on C-G can be isolated or in intersecting networks creating polygonal patterns [*El-Maarry et al*., 2015a]. Polygons, when present, are ~1–5 m wide. Fractures are also observed on cliff walls, scarps, and even on large (20–30 m wide) boulders.

These different fracture settings and topologies prompted *El-Maarry et al*. [2015a] to suggest that multiple formation mechanisms were responsible for fracturing the nucleus surface. However, they concluded that thermal insolation weathering was currently the main driving mechanism, along with possibly seasonal thermal contraction of ice-rich near-subsurface material. In addition, comet C-G displays unique isolated fracture systems such as a long ($>$500 m) single fracture running through the northern neck region (Figure 2e), which may suggest that tectonic influences (orbital, gravity, or sublimation induced) are also playing a role in fracturing the comet [*El-Maarry et al*., 2015a].

Fractures appear to be driving other processes as well, such as mass wasting and possibly jet activity. In particular, fractures are observed on the edges of cliffs and scarps, which also display talus deposits at their base, indicating that fractures are acting as drivers for cliff collapse and ensuing mass wasting (see section 4). In addition, *Vincent et al*. [2016] suggest that fractured cliffs are one of the main sources of dust jets, which are accelerated inside the fractures, and imply that the same mechanism may be taking place on all other active comets [see also *Farnham et al*., 2007, 2013].

In light of the observations at C-G, it may be possible to identify candidate fracture patterns on the other comets even in lower resolution images. Features that were commonly described as layers may be unresolved fractures. While no obvious candidates for fractures can be seen in images of Wild 2, Borrelly, or Hartley 2, the thick linear layers of Tempel 1 (Figure 2h), as previously interpreted by *Thomas et al*. [2007], might be consistent with fractures similar to those observed at much higher resolution in C-G's cliffs (Figure 2f). Differences in lighting illumination and resolution complicate any direct comparisons. However, images of C-G were acquired by Rosetta's navigation camera under conditions more similar to those at Tempel 1 (Figure 2g). It is clear that the smaller crosscutting components of fractures seen on C-G, if present, would not be resolved in the Tempel 1 images. These comparisons suggest the possibility that what appears to be layers on Tempel 1 could be fracture systems, illustrating that caution should be used in assigning specific origins to features observed at only modest resolution.

4. Sedimentary Processes

Sublimation of ices and the resulting gas lift dust from the surface. In a cometary context, dust thus refers to material of any size that is or was physically detached from the nucleus. Any dust not accelerated to escape velocity, typically in the centimeter and decimeter size range for active comets, can fall back to the nucleus providing a mechanism for movement of material and, in particular, a potential means of producing smooth surfaces on nuclei. This process was discussed by *Möhlmann* [1994], who suggested that it may be responsible for the production of a loosely packed "deposition regolith" particularly on inactive regions. Nonetheless, it was somewhat unanticipated when such sedimentary processes began to be resolved on cometary nuclei. A hint was first seen on Halley, which contained a smooth central depression, albeit

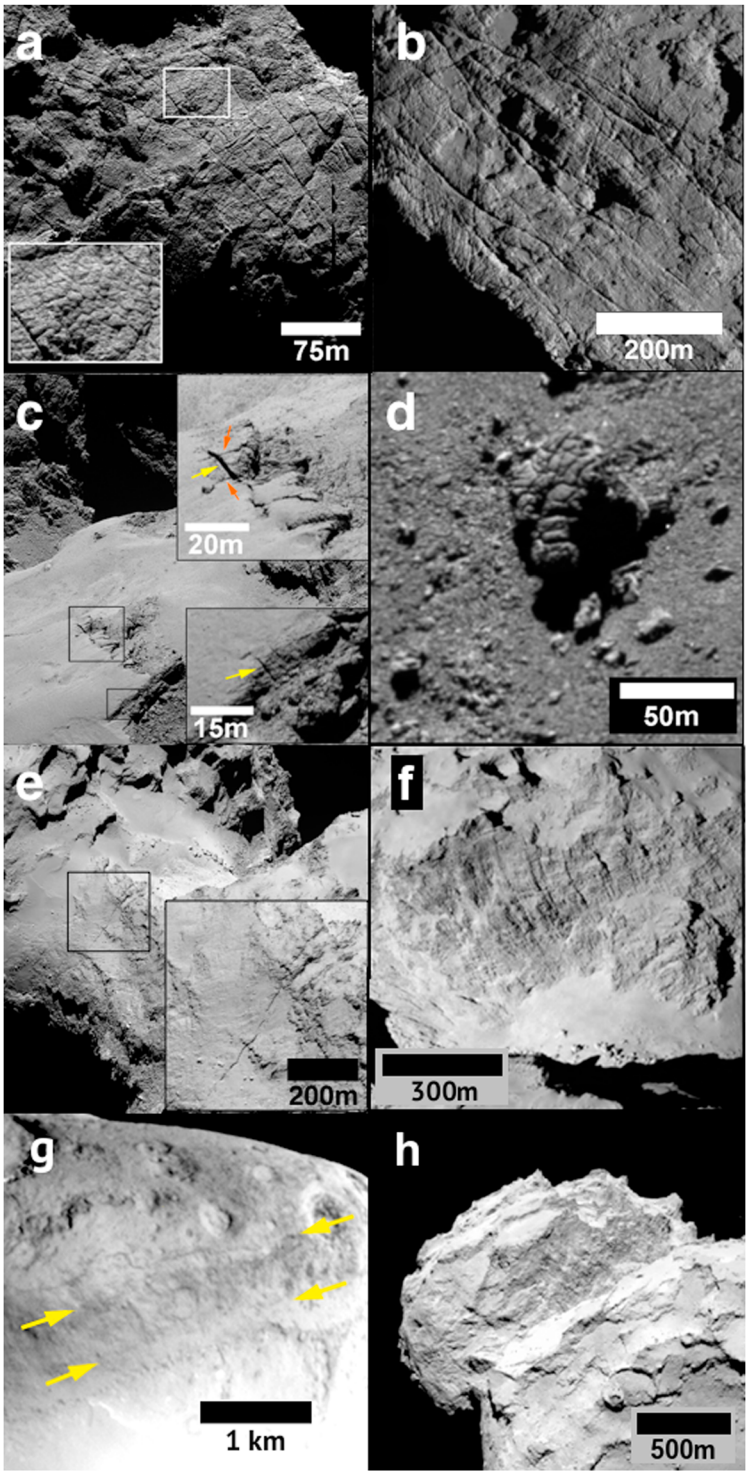

Figure 2. Fractures on comet C-G (a–f) Fractures on comet C-G and (g) candidate fractures on Tempel 1. (a) Polygonal fracture patterns at the boundary between the Northern and Southern Hemispheres of the large lobe. (b) Long <300 m long fractures on the Southern Hemisphere of the small lobe. (c) Fractures on escarpments. Higher resolution images are inset. (d) Fractured boulder on the Northern Hemisphere. (e) Approximately 500 m long fracture running through the neck of C-G. (f) The 900 m high cliff on C-G on the small lobe above the neck region that includes a set of aligned perpendicular linear features. From *Thomas et al*. [2015a]. (g) Parallel layers on Tempel 1 from *Thomas et al*. [2007]. (h) C-G cliffs in Figure 2f, acquired with the NAVCAM (ROS_CAM1_20140815T020718F) at a resolution and under illumination conditions more similar to the features imaged on Tempel 1 (Figure 2g). These images suggest that the layered terrain on Tempel 1 may potentially have the same fracture origin as the cliffs resolved in much greater detail on C-G. Figures 2a and 2c–2e are adapted from *El-Maarry et al*. [2015a].

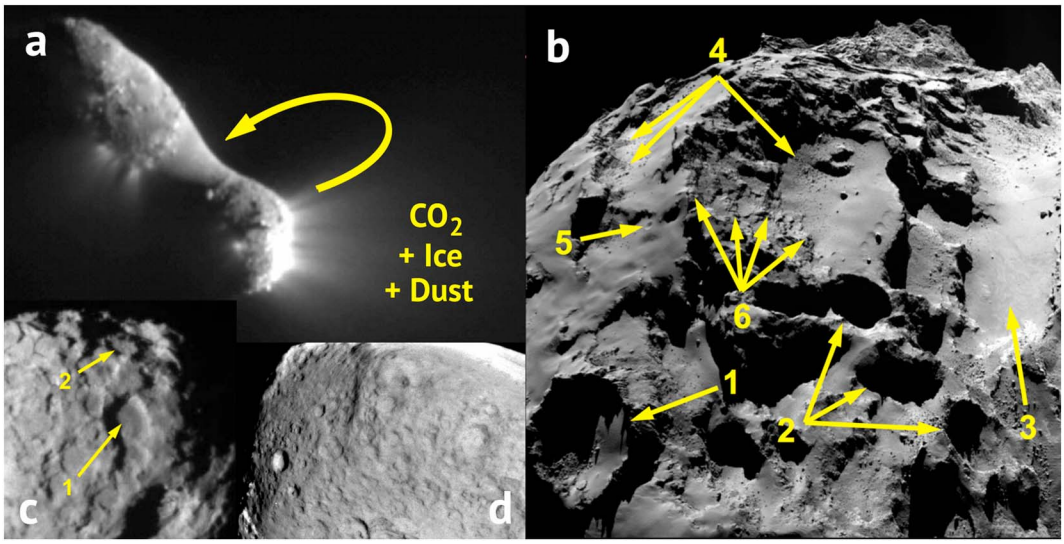

Figure 3. (a) Hartley 2. After *A'Hearn et al.* [2011]. (b) A variety of morphologic features on C-G as observed in this wide-angle image acquired from 10 km above the center of the nucleus. The image shows a possible large impact crater (1), a smaller crater (5), active pits (2), the inferred more active smooth region (3), and talus at the base of vertical cliffs (4). The edge of the depositional layer is also indicated (6). (c) Flat-floored craters (1) and pit-halo features (2) on Wild 2. From *Brownlee et al.* [2004]. (d) Pits and depressions observed on Tempel 1 observed by Stardust NExT. From *Thomas et al.* [2013a].

observed at relatively low resolution [*Keller et al.*, 1986]. The presence of smooth regions on Tempel 1 was the first suggestion of large-scale movement of material on comets [*A'Hearn et al.*, 2005; *Thomas et al.*, 2007]. However, it was Hartley 2 [*A'Hearn et al.*, 2011], where evidence for mass movement of material across a cometary nucleus as an ongoing process was first revealed. Infrared spectroscopy revealed that the small, very active end of Hartley 2 emitted CO_2 gas, dragging both dust and water ice grains from the nucleus (Figure 3a). The smooth waist of Hartley 2 also had enhanced emission of water vapor. This led *A'Hearn et al.* [2011] to suggest that ice grains dragged from the end of the nucleus by CO_2 would likely fall back to the gravitational low of the waist. Subsequent analysis of the flyby images of Hartley 2 showed individual icy chunks in the coma could be tracked and that many were traveling below the escape velocity and were therefore in orbit and would eventually redeposit on the surface [*Hermalyn et al.*, 2013].

The early observations of C-G have provided considerable support for this concept. *Thomas et al.* [2015a] showed that a significant fraction of the northern hemisphere was covered with a thin ($<$5 m thick) coating of material whose source may potentially be in the active neck region (Figure 3b). The southern hemisphere, active near perihelion, has also been predicted to be a major contributor providing a means of transport of nonvolatile material from south to north [*Keller et al.*, 2015]. The lack of a substantial dust covering in the Southern Hemisphere [*El-Maarry et al.*, 2016] may also be the result of this more vigorous outgassing. *Rotundi et al.* [2015] identified substantial quantities of centimeter- to decimeter-size dust particles in bound orbits, and *Thomas et al.* [2015b] showed the presence of slow-moving individual particles immediately above the surface. This form of sedimentation, variously described as "air fall" or as a "dust hail," is clearly a means of producing layers on the nucleus that can vary in depth in response to the orbital evolution of the comet (e.g., Figure 3b6).

A remarkable observation from C-G was the discovery of "ripples" in the dust layer in the neck of the nucleus. (The smooth region within the neck is indicated in Figure 3b3.) The morphological similarity to aeolian ripples is striking including the amplitude/wavelength ratio of 0.02–0.04 [*Thomas et al.*, 2015b]. A key problem with this interpretation is that gas densities at the surfaces of cometary nuclei can be 5 orders of magnitude lower than on, for example, Mars even where the comet is active. In addition, gas outflow is often assumed to be mostly radial. However, both modeling [e.g., *Kitamura et al.*, 1985] and observation [e.g., *Keller and Thomas*, 1988] have long suggested that nonradial components of outgassing can be substantial if gradients in surface activity are large. It should be noted that such gas-driven mechanisms are fundamentally different

from typical aeolian processes in that the gas on comets originates from the surface itself, not as a near-surface atmospheric effect.

Thomas et al. [2015b] showed that "cometary saltation" may be feasible for centimeter-sized particles and recent work by *Pähtz and Durán* [2016] has provided additional support for this hypothesis. Gas number densities at the surface reach of order 10^{-17} m^3 for production rates of 1–2 kg/s and are therefore modest but can easily be 2 orders of magnitude higher. This can increase further from even weak confining pressures. For example, *Thomas et al*. [2015b] used a gas pressure of 3–30 nbar and showed that the neck could act as a weakly confining tube where velocities of ~500 m/s could then be achieved close to the surface. Smaller particles, which have may have interparticle cohesive forces that hinder their movements [*Kührt and Keller*, 1994], may also become mobile after interactions with larger particles that do not escape the nucleus. Other features on the nucleus of C-G have been hypothesized as being the result of gas-driven particle motion including putative wind tails and aligned dune-like structures [*Thomas et al*., 2015b], although detailed modeling remains to be performed. However, alternative explanations, including the effects of subsurface topography, should not be excluded. In several places on C-G, the surface texture differs from one side of a boulder to another. A smooth texture may be seen on one side and a rougher texture on the other. There are two related explanations that are both connected to gas-driven particle motion. *Thomas et al*. [2015b] suggested that the smoother materials might be "wind tails" from near-surface flow of a gas-dust mixture, where particles would be deposited behind an obstacle as a result of the fluid flow of dust-laden gas around it. In contrast, *Mottola et al*. [2015] modeled the abrasion from reimpacting particles and concluded this mechanism is responsible for the observed formations.

Further evidence of dust transport is seen in the presence of ponded deposits on C-G [*Thomas et al*., 2015b] similar to those previously observed on the asteroid 433 Eros [*Robinson et al*., 2001]. There appears to be increasing evidence for electrostatic levitation and transport of dust on airless bodies [e.g., *Poppe et al*., 2012], and this is probably the favored mechanism here. For electrostatic lofting, cohesive forces need to be accounted for, which leads to preferential lifting of intermediate-size (15 μm) grains [*Hartzell et al*., 2013], but this potential problem may not exist for comets because sublimation contributes to the grain levitation [*Thomas et al*., 2015b]. Alternative ponded deposit production mechanisms including seismic shaking [*Cheng et al*., 2002], disaggregation of boulder material [*Dombard et al*., 2010; *Roberts et al*., 2014], near-surface fluidization [*Sears et al*., 2015], and micrometeoroid impact [*Colwell et al*., 2005] have been investigated and may also be plausible.

4.1. Collapse and Mass Wasting

The association of activity with vertical cliff faces was first observed in Deep Impact images along the distal scarp of the large smooth flow on Tempel 1 [*Farnham et al*., 2007]. Jet activity from a cluster of seven jets was also correlated to the walls of terraces on the Stardust NExT side of Tempel 1 [*Farnham et al*., 2013]. On C-G, there are numerous sites showing evidence of undercutting and collapse at near-vertical surfaces [*Thomas et al*., 2015a]. The sedimentation of dust may participate in this process by acting as an insulating layer on the horizontal surface of an outcrop or cliff, while the vertical face remains exposed to sunlight and therefore is active. *Vincent et al*. [2016] have presented evidence for activity associated with cliffs, and *El-Maarry et al*. [2015a] suggest that fractures drive cliff collapse and mass wasting processes that eventually lead to the formation of talus deposits at the bases of cliffs, which are common features in C-G's weakly consolidated regions (see Figure 3b4). It is likely that the blocks in the talus continue to fracture and erode, ultimately leaving behind the smooth dust layers that are seen farther from the cliff edges [*Pajola et al*., 2015].

5. Large-Scale Flows

Among the most enigmatic landforms seen on the surfaces of any comet are the large smooth deposits on Tempel 1 [*A'Hearn et al*., 2005]. Tempel 1 as observed by Deep Impact contains three probable flows (S1–S3 in Figure 4a) each of which lies in a topographic low and extends over several square kilometers in area [*Thomas et al*., 2007]. A fourth laterally confined likely flow was observed on the regions of Tempel 1 imaged only by Stardust NExT [*Thomas et al*., 2013a]. The largest and most prominent (S1) shows morphologic evidence of flow (see Figure 4b) and ends in a >20 m scarp [*Thomas et al*., 2007], which has also been shown to be a source of cometary activity [*Farnham et al*., 2007]. The large S1 flow first discovered in 2005 by Deep Impact was observed again in 2011, a full orbit (5.5 years) later, by Stardust NExT [*Veverka et al*., 2013]. The

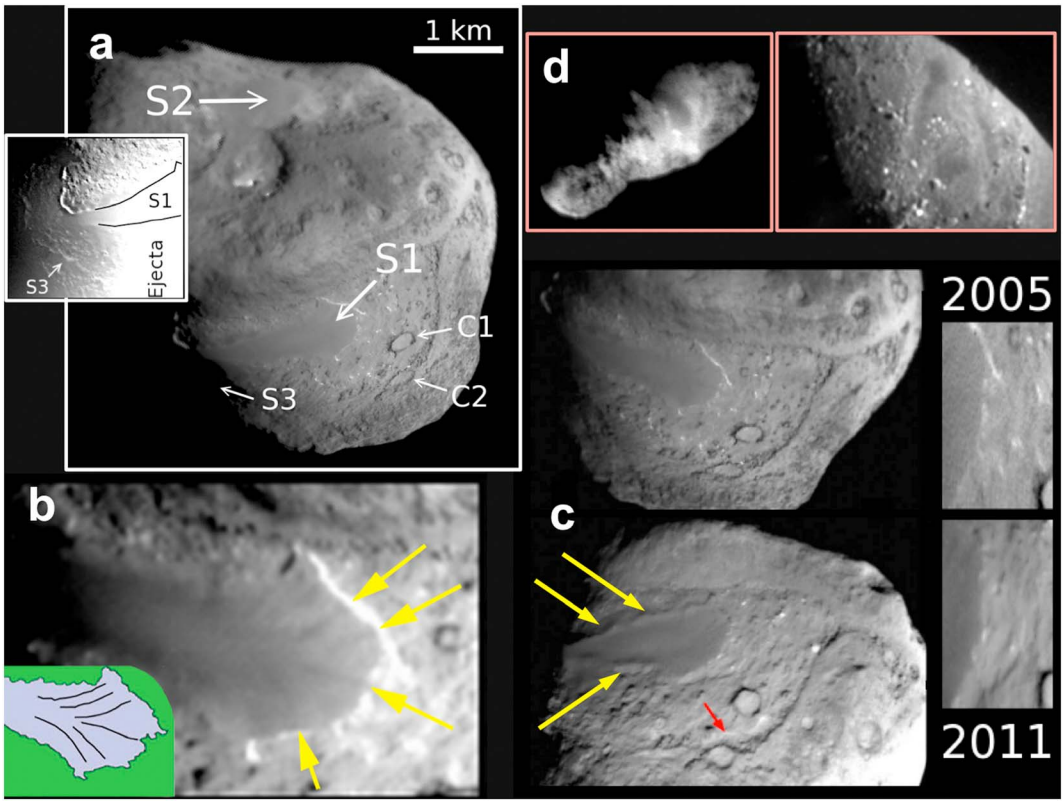

Figure 4. Several kilometer-scale smooth flows exist on Tempel 1. (a) Three large smooth flows (S1–S3) on Tempel 1 as imaged by Deep Impact in 2005. The inset shows the details of S3 in the terminator region as indirectly illuminated by scattered light from ejecta generated by the Deep Impact experiment. C1 and C2 denote 300 m diameter circular features with raised rims that are the mostly likely candidate impact craters observed on comets as discussed in section 8. (b) High-pass filtered image emphasizing flow-like textures and the terminal scarp of the S1 flow. After *Thomas et al.* [2007]. (c) Comparison of the S1 flow on Tempel 1 seen by Deep Impact in 2005 and one orbit later by Stardust NExT in 2011. Retreat of the scarp is seen in the subimages, which are rectified to remove first-order geometric effects. The red arrow denotes the Deep Impact experimental impact site. Yellow arrows denote terminal levee-like features seen by Stardust NExT. After *Thomas et al.* [2013a]. (d) Candidate flow features seen on other comets: (left) the smooth dark region on Borrelly [*Soderblom et al.*, 2002] and (right) smaller smooth features on Hartley 2 [*A'Hearn et al.*, 2011]. Large smooth flows are inexplicably absent on Wild 2 and the well-mapped C-G.

viewing geometry of the 2011 images reveals morphologies along the margins that are suggestive of levees (Figure 4c) [*Thomas et al.*, 2013a]. Furthermore, the flow's scarp showed signs of evolution between the two encounters, with edges that retreated in places up to 50 m and pits along the edge that collapsed, with a total loss of nearly 2×10^8 kg of material [*Thomas et al.*, 2013a].

Belton and Melosh [2009] explored the possibility that the Tempel 1 flows were cryovolcanic (i.e., fluid) by invoking an exothermic phase transition of subsurface ice from amorphous to crystalline form [e.g., *Prialnik*, 1997]. The catastrophic release of heat fluidizes the cometary material, which is then driven from depths of ~100 m to the surface. Based on their proposed phase transition from amorphous ice, which is thought to be typical in cold cometary formation regions, *Belton and Melosh* [2009] predict that cryovolcanic flows should be common on comets. In addition, they expect large internal voids to be present after material has been released.

However, such large smooth flows as observed on Tempel 1 are not common on comets. Although it was originally interpreted as a mesa [*Britt et al.*, 2004], a large kilometer-sized dark band was seen on Borrelly Figure 4d that, at the resolution imaged, is also consistent with a smooth flow in a topographic low [*Thomas et al.*, 2013a]. At smaller scales, smooth regions on Hartley 2 (Figure 4d) may also be flows [*A'Hearn et al.*, 2011]. Most surprisingly, kilometer-scale smooth deposits with flow-like morphologies are entirely absent on C-G despite the high resolution and complete mapping of Rosetta at 10 m scales. Large

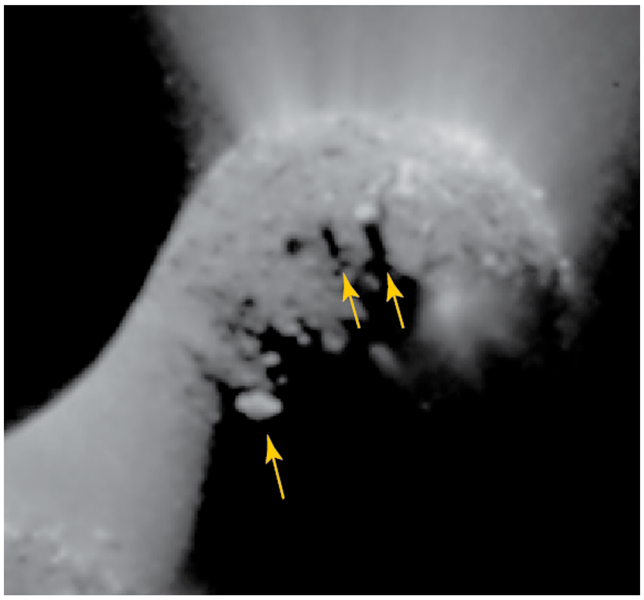

Figure 5. Tall spires, unique to Hartley 2, the most active comet visited to date, are among the rare cometary landforms that are likely associated with jetting. See Figure 2 in *Bruck-Syal et al*. [2013].

flow-like deposits in topographic lows are also absent on Wild 2. As for potential internal voids within the nucleus, at the scale of 10–100 m, both the gravity [*Pätzold et al*., 2016] and moment of inertia measurements [*Sierks et al*., 2015] of C-G are consistent with a homogeneous nucleus. Furthermore, the Comet Nucleus Sounding Experiment by Radiowave Transmission (CONSERT) bistatic radar experiment between the Rosetta orbiter and lander that propagated 560 and 760 m through the small lobe C-G did not detect any density variations down to scales as low as 3 m [*Kofman et al*., 2015]. Given the discrepancy between the model predictions inferred from Tempel 1 and observations of C-G, it remains unclear if the *Belton and Melosh* [2009] cryovolanic mechanism can explain the large flows.

Although much smaller in scale (hundreds of meters) and morphologically different, a smooth region on C-G has been observed to show significant change over timescales of days [*Groussin et al*., 2015]. The upper ~5 m of surface is seen to collapse in circular wave-like structures that propagate across the surface. Embayment at some unit boundaries is consistent with a flow origin [*Thomas et al*., 2015a]. However, the responsible mechanism for this terrain may not be a flow but rather a continuous fluidization of the surface layer. This and other potential processes (e.g., solid or glacial flow) need to be explored and tested more rigorously against the morphology observed (e.g., the levees). In addition, it is unclear why Tempel 1 has multiple large flows, while C-G has none even though both comets have broadly similar sizes, and orbits, and overall activity rates. Determining the origin of the flow-like features, both large and small, may lie in understanding this enigma.

6. Landforms Associated With Jets

Given the dramatic evidence of outgassing seen in dust jets from all active comets, it is very surprising that very few direct expressions of jetting on cometary surfaces have been identified. In particular, no morphologies consistent with proposed vent mechanisms [e.g., *Sekanina*, 1991] have been observed on any comet [e.g., *Vincent et al*., 2016]. In addition, as discussed below, there are only a few examples of landforms that might be sculpted by jet activity. Associating specific landforms with jet activity is hampered by the difficulty in observing optically thin dust against a relatively bright nucleus, a general lack of understanding of dust activity, and the fact that there are no terrestrial analogs. Yet all comets show local enhancements in the dust coma that can be traced back, somewhat imprecisely, to specific regions [*Farnham et al*., 2007, 2013; *Vincent et al*., 2016].

Highly localized jets have been associated with landforms in two specific cases. The clearest examples are the tall spires (Figure 5) observed by Deep Impact during its flyby of Hartley 2 [*Thomas et al*., 2013b; *Bruck-Syal et al*., 2013]. These overhung mounds are tens of meters wide with long shadows indicating that they extend 40–60 m above the surface. These spires are unique to Hartley 2, the most active comet visited to date, which suggests they may be linked to outgassing. They could be relic features that remain after erosion that are somehow more coherent than the surrounding material (i.e., akin to resistant hoodoos), or they could be formed as part of the jetting process [*Bruck-Syal et al*., 2013]. While there are suggestions of other associations of jet activity with rough blocky terrain on Hartley 2 [*Bruck-Syal et al*., 2013], identification of specific landforms is hindered by the fast flybys and limited spatial resolution. On C-G, *Vincent et al*. [2015] observed activity directly inside pit-like depressions hundreds of meters in diameter (see section 7).

7. Depressions and Pits

7.1. Quasi-Circular Depressions

Quasi-circular depressions are common on cometary surfaces. *Brownlee et al*. [2004] defined two types of depressions from the Stardust observations of Wild 2: flat-floored/steep cliff structures and "pit-halo" features, which are rounded central pits surrounded by an irregular and rough region of partially excavated material (Figure 3c). To date, such pit-halo structures appear to be unique to Wild 2. Flat-floor depressions however are more common. For example, the northern lobe of one of the flat-floored depressions on Wild 2 (Left Foot) is 650 m across and 140 m deep with walls that are nearly vertical (>70°) in places making sharp contact with the flat floor [*Brownlee et al*., 2004]. *Brownlee et al*. [2004] also observed some rubble at the base of cliffs. Similarly circular depressions seen on C-G's northern weakly consolidated regions suggesting similar production mechanisms on Wild 2 and C-G [*Thomas et al*., 2015a]. *Thomas et al*. [2013a] also noted the presence of "crisp steep-walled pits" on Tempel 1, a few having flat floors (Figure 3d). In all cases, there is no visible evidence of any ejecta.

These depressions can be distinguished from other circular pits. *Brownlee et al*. [2004] note that the flat-floored depressions on Wild 2 were inactive and no evidence of activity from the examples on C-G has been reported to date. However, *Vincent et al*. [2015] showed that some pits (up to ~170 m in depth) adjacent to the depressions on C-G with near vertical sides were actively emitting dust from their sides (Figure 3b2).

The mechanisms that produce depressions on the surfaces of comets are unclear. It is likely that different types of depressions have different origins. Possible mechanisms include collapse of interior voids [*Vincent et al*., 2015], impact into a porous medium [e.g., *Housen and Holsapple*, 2012] possibly with a more cohesive surface layer [*Brownlee et al*., 2004], and sublimation processes possibly including episodic outbursts [*Mousis et al*., 2015].

7.2. Irregular Depressions

Ground-based observations indicate that intermittent large-scale mass loss and splitting of cometary nuclei are relatively common [e.g., *Chen and Jewitt*, 1994; *Boehnhardt*, 2004; *Fernandez*, 2009]. C-G shows depressions, which might be the result of large-scale mass loss [*Thomas et al*., 2015a]. In particular, one of the large (0.12 km^3) irregular depressions in the large lobe of C-G (Figure 6) appears to be surrounded by weakly consolidated, dust-coated materials from neighboring regions [*Thomas et al*., 2015a]. However, the interior of the depression shows no evidence of a similar dust coating [*El-Maarry et al*., 2015b]. At the edges of the depression, disrupted weakly consolidated material is seen, suggesting a recent formation.

8. Impact Cratering

Cometary nuclei, in general, are devoid of craters that are of obvious impact origin. This is in sharp contrast to inactive surfaces such as asteroids, where the overall shape and dominant surface geology is a record of impact collisions throughout their history [e.g., *O'Brien et al*., 2006]. A paucity of impacts is consistent with young surface age as is expected from sublimation-driven erosion of these comets since they entered the inner Solar System. It may also reflect the difference in impactor populations and velocities between the Asteroid Belt and the outer Solar System.

There are, however, a few features on the surfaces of well-resolved cometary nuclei that could plausibly be impact in origin. On C-G there is a 35 m diameter structure (Figure 3b5) that is interpreted as a semiburied crater [*Thomas et al*., 2015a] used to estimate the depth of the dust deposits in the northern hemisphere. In addition, three other structures are observed on C-G that might be impact related. In all three cases, the surroundings are deflated (e.g., Figure 3b1). Compaction by impact can lead to lower volume loss locally (if sublimation is the main erosional process) giving the appearance of pedestal-like craters. This warrants further investigation and detailed modeling as it may place constraints on surface age and previous history.

The best examples of potential impact craters on comets are the two circular depressions that were imaged by Deep Impact on comet Tempel 1 (C1 and C2 in Figure 4a). These ~300 m diameter features appear to have raised rims. (Ironically, these putative impact craters flank the Deep Impact experimental impact site; see Figure 4c.) The presence of these two large craters on a cometary nucleus is enigmatic. They imply a

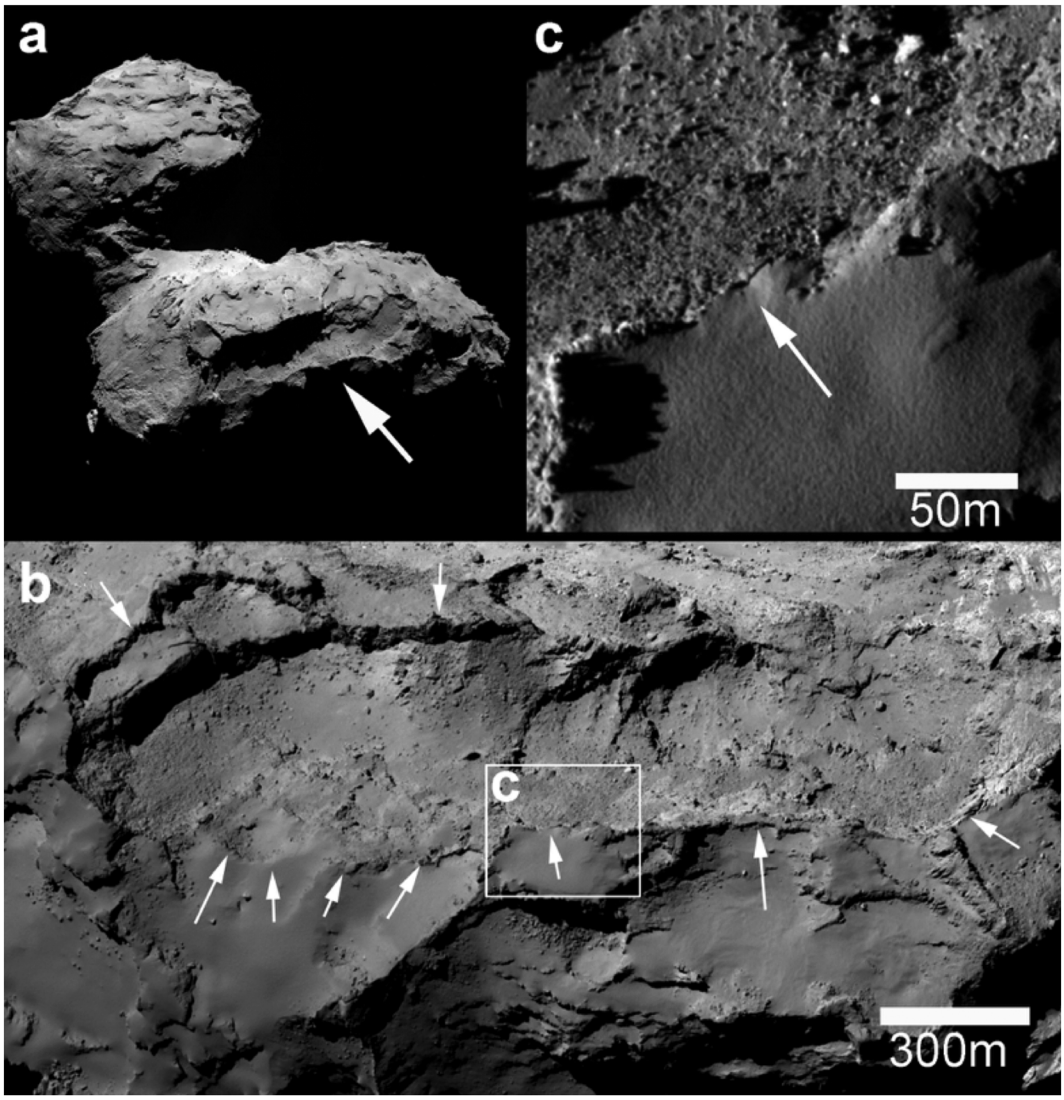

Figure 6. A large irregular depression is seen on C-G. (a) Location on the large lobe. (b) Detailed view of the depression. Talus-like deposits caused by collapse of rim materials appear to cover parts of the depression, but no smooth deposits are observed in the interior. The box shows the position of the region expanded in. (c) The different morphologies in the depression's interior and rim. Adapted from *El-Maarry et al*. [2015b].

population of relatively large impactors and thus relatively old ages, which are difficult to preserve on an active comet. Given the high porosity of comets (section 2), any reasonably high velocity impact would penetrate deeply and produce substantial compression [e.g., *Schultz* et al., 2007]. As such, the present circular features may be relics of that compression and may be preserved parts of the crater that were significantly below the original impact surface. It is equally puzzling to find possible impact craters on only one comet and in only one location. One rationale may be that these relatively large craters occur in a region that likely was covered by Tempel 1's large smooth flow (S1), which is itself unique and may have helped preserve the morphology of the craters.

9. Terraced Terrains

Arguably, the most ubiquitous surface features on comets are their terraced terrains, which are clearly seen on Wild 2, on both sides of Tempel 1, and dominate C-G (see Figures 1, 4a, and 7a). Most notably, the terraces are observed at every scale imaged on comets: over hundred of meters, for example, on the side of Tempel 1

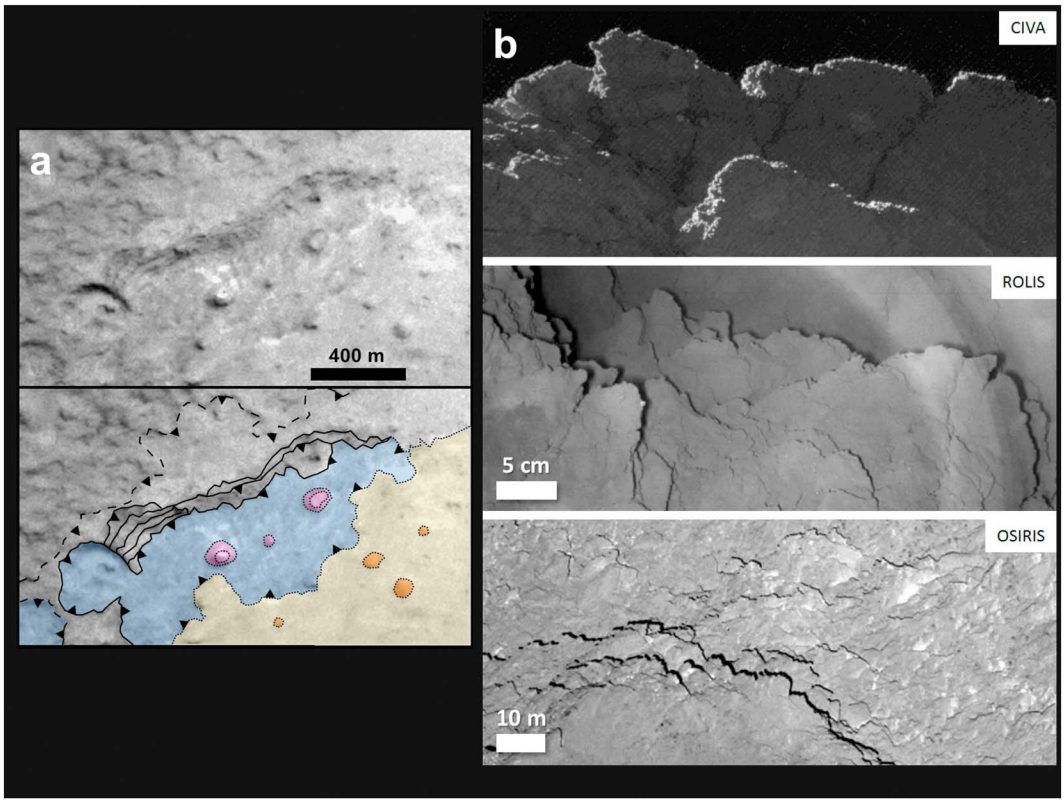

Figure 7. Terraced terrains on comets are observed over a broad range of scales and are remarkably similar. (a) Terraces on Tempel 1 as seen in images from Stardust NExT [*Thomas et al*., 2013a] are kilometers in length and, in total, span 50 m in relief. (b) From *Schroeder et al*. [2016]. The self-similarity of terraces at all scales is accentuated at near zero-phase angles where shadowing is minimized. Optical, Spectroscopic, and Infrared Remote Imaging System (OSIRIS) Narrow Angle Camera images of C-G acquired from the Rosetta Orbiter at 0.9° phase and 11 cm/pix are compared to orders of magnitude higher resolution images taken from the Philae lander under LED lighting (~0° phase) with the down-looking ROLIS camera at ~1 mm/pix [*Mottola et al*., 2015] and nearby in cliffs seen from side-looking CIVA images [*Bibring et al*., 2015]. The distance to the cliffs and thus the exact scale of CIVA images is unknown but is mm-cm/pix.

imaged by Stardust NExT [*Thomas et al*., 2013a], to the millimeter-scale images from the Philae lander cameras [*Bibring et al*., 2015; *Mottola et al*., 2015]. As shown in Figure 7 and discussed by Schroeder et al. (Close-up images of the final Philae landing site on comet 67P/Churyumov-Gerasimenko acquired by the Rosetta Lander Imaging System (ROLIS) camera, submitted to *Icarus*, 2016), images taken near zero-phase angle, where shadows are repressed, accentuate the long, arcuate terraced textures. These zero-phase images are nearly identical to those obtained from 6 km above the surface (11 cm/pix) at 0.9° phase with Rosetta's orbiter camera (Figure 7b) and acquired at low (near zero) phase under light-emitting diode (LED) illumination with the down-looking camera ROLIS from the surface [*Schroeder et al*., 2016]. Similar terraced terrains are evident (Figure 7b) in cliffs imaged at cm-mm/pix in the side-looking Comet Infrared and Visible Analyser (CIVA) images from the Philae lander [*Bibring et al*., 2015]. At global scales, the terraces of Tempel 1, imaged ~10 m/pix, are seen to extend over km lengths (Figure 7a) [*Thomas et al*., 2013a]. The individual terraces are at the resolution limit of the images, but are likely 10–15 m high providing a total vertical relief of some 50 m.

The origin of these terraced terrains remains controversial as several different mechanisms may contribute to their formation, including layering during the formation of cometesimals, sedimentary deposits from mass movement of materials, and retreating fronts from sublimation. *Belton et al*. [2007] suggested that layering on comets, particularly what was thought to be thick layers observed on Tempel 1, is caused by accumulation of slow velocity highly porous cometesimals, which flatten on impact. Subsequent hydrocode modeling showed that such pancake impacts are possible given the weak tensile strength of comets [*Jutzi and Asphaug*, 2015]. Under this layer pile model, the terraces observed on the surfaces of comets reflect their internal structure. It is notable that the layered impact model was envisioned to explain Deep Impact images

of Tempel 1, which were originally interpreted to be parallel layers [*Thomas et al*., 2007]. However as discussed in section 3 (Figures 2f–2h), comparisons to the high-resolution images of C-G suggest the Tempel 1 layers could be similar to the cliffs above the neck region on C-G and may therefore be poorly resolved sets of joints. As described in section 4, it is also clear from images of C-G (see Figures 3b and 6c) that deposition of dust can produce deposits that are tens of meters thick and also create terracing on cometary surfaces. Finally, activity from sublimation has been documented to occur on vertical surfaces (see section 4), which in turn leads to undercutting and downslope movement of material. Over time, the backwasting will also produce terraces.

All three of these processes may contribute to layering on comets. However, the ubiquitous nature of terraces and their self-similar occurrence from centimeters to hundreds of meters argues for a common process that occurs at all scales. Neither depositional layers nor accretion via pancake impacts [*Belton et al*., 2007] are compatible with the terracing observed on comets at all scales, particularly at scales of centimeters or less. Sublimation, however, is expected to occur at all scales. Terraced surfaces can be created on comets through a combination of changing thermal conditions and inhomogeneities in strength created by local recondensation and small-scale variations in abundances of ice and refractories, or porosity. Thermal variations occur cyclically on diurnal and annual scales, which propagate to depths of several centimeters and decimeters, respectively [*Groussin et al*., 2013]. Given the colder near surface of comets, the ensuing sublimation drives gas into the interior where it recondenses to produce a structurally and chemically inhomogeneous layer often referred to as the KOSI-layer after similar effects in laboratory experiments [*Kochan et al*., 1998; *Poch et al*., 2016]. It should be noted that the details of many of these processes as they pertain to actual cometary surfaces remain poorly known. Thus, while sublimation-driven backwasting due to variations in insolation and strength is a mechanism that could produce the widespread terracing observed on comets at all scales, it is far from proven.

10. Conclusions and Summary

Cometary nuclei have proven to be complex and fascinating geologic worlds with unexpected physical processes acting to alter their surfaces. The wealth of observations of the six nuclei visited by spacecraft has revealed a diverse population far more complex than expected. Any semblance that comets are simply dirty snowballs is no longer tenable. Comets exhibit a variety of overall shapes, most of which are bilobate, providing strong evidence that they were formed from smaller cometesimals. The surfaces of comets contain a heterogeneous set of morphologic landforms that vary across both individual bodies and among different nuclei. It is somewhat surprising that on scales of the various morphologic features seen on comets, no obvious compositional variability is observed. It also remains largely unclear why certain geologic processes, for example, those that form large kilometer-scale flows on Tempel 1 or tall spires on Hartley 2, are active on some comets but not on others. Insolation, which varies on daily, seasonal, and geologic timescales and is dependent on a comet's rotation, pole position, and topography, must be a major factor in why geology varies from comet to comet, but it is unlikely to be the only cause. Insolation-driven sublimation is expected to contribute significantly to cometary landforms. Sublimation from near-vertical faces has been documented on many comets. In higher resolution data of comet C-G, this is seen to lead to material wasting and collapse. Backwasting from sublimation along strength inhomogeneities from near-surface recondensation or sintering [e.g., *Grün et al*., 1993; *Kossacki et al*., 1997; *Kochan et al*., 1998] is also the mechanism that appears to best explain terraced terrains observed on multiple comets and at scales ranging from millimeters to hundreds of meters. Yet our understanding of the basic relationship between large- and small-scale surface roughness, local heating of the surface, and their link to outgassing remains unclear.

Several unexpected processes are now seen to be significant on comets. Because of the low escape velocities on these small bodies, prior to the most recent data from Hartley 2 and C-G, the role of particle fallback and associated sedimentary processes, particularly mass movement of material, was severely underestimated. While the transport of material across the nucleus is now recognized as an important process, likely dominated by gas-driven mobility, other effects such as electrostatic forces might be influencing the appearance of surface deposits.

Similarly, the low strength and high porosity of cometary surfaces was not anticipated to sustain fractures, yet fractures are seen to be ubiquitous at all scales in the high-resolution images of C-G. Inhomogeneities in

strength at local scales may be necessary to support such fracturing. The presence of near-surface volatiles could play a role, particularly in sintering processes that act to harden the near-surface layers [e.g., *Grün et al*., 1993; *Kossacki et al*., 1997; *Pommerol et al*., 2015; *El-Maarry et al*., 2015a]. Indeed, recent results from instruments on the Philae lander [*Spohn et al*., 2015; *Lethuillier et al*., 2016] suggest variations in thermal inertias and increased material strengths at depths of tens of centimeters. Thermal shock and fatigue are major drivers of fractures. However, the unusual conditions on comets (microgravity, high porosity, and low strength) may also balance in such a way to facilitate fracturing and other processes.

While comets are compositionally primitive bodies, they are among the most geologically active. The retreat of a scarp on a smooth flow on Tempel 1 between the flybys of two different spacecraft was the first documentation of changes on an orbital timescale of a cometary nucleus [*Veverka et al*., 2013]. Changes have been detected over many different timescales on C-G, including as short as hours in one region [*Groussin et al*., 2015]. As Rosetta continues to move with the comet past perihelion, its ongoing observations, particularly those showing dust production from the southern hemisphere and subsequent deposition in the Northern Hemisphere, will allow further documentation and quantification of surface evolution. It is also notable that the highest resolution images of C-G will be collected around the end-of-mission landing in September of 2016. These new data will provide additional constraints on various processes and their timescales and will undoubtedly raise new sets of questions.

It is now clear that cometary geomorphology is an established discipline. However, much about these intriguing worlds remains enigmatic. Future efforts must reconsider our intuition of how geologic processes work in cometary environments of near-zero gravity, low strength, and high porosity. In addition, there are surface structures on all comets, from the flat-bottomed depressions on Wild 2 and C-G to the spires of Hartley 2, for which we do not understand the production mechanisms—even to a first order. Similarly, research needs to focus on why certain landforms and processes occur on some comets and not others. Perhaps the most extreme example of this is the existence of numerous kilometer-scale flows on Tempel 1 and their complete absence on C-G despite broad similarities in the two comets' bulk size, age, and activity levels. Unraveling the origin and evolution of cometary surfaces will require further synthesis of existing data and new data yet to be acquired by Rosetta. In addition, progress on these outstanding issues will require the modeling and quantification of processes on cometary surfaces, which are currently described only qualitatively, the incorporation of the knowledge gained from laboratory studies, specifically those focused on sublimation under cometary conditions, and comparisons of similar processes in other geologic environments.

Acknowledgments
Funding to M.R.E. and N.T. from the Swiss National Science Foundation through grant 200020_165684 and to TLF from NASA's Planetary Mission Data Analysis Program through grant NNX12AQ64G is gratefully acknowledged. Data from cometary missions can be found in NASA's Planetary Data System (PDS) Small Bodies Node (SBN) http://pdssbn.astro.umd.edu and/or ESA's Planetary Science Archive (PSA) http://www.rssd.esa.int/index.php?project=PSA.

References

A'Hearn, M. F., et al. (2005), Deep impact: Excavating comet Tempel 1, *Science*, *310*, 258–264.
A'Hearn, M. F., et al. (2011), EPOXI at comet Hartley 2, *Science*, *332*, 1396–1400.
A'Hearn, M. F., et al. (2012), Cometary volatiles and the origin of comets, *Astrophys. J.*, *758*, 29.
Basilevsky, A. T., and H. U. Keller (2006), Comet nuclei: Morphology and implied processes of surface modification, *Planet. Space Sci.*, *54*, 808–829.
Belton, M. J. S., and J. Melosh (2009), Fluidization and multiphase transport of particulate cometary material as an explanation of the smooth terrains and repetitive outbursts on 9P/Tempel 1, *Icarus*, *200*, 280–291.
Belton, M. J. S., et al. (2007), The internal structure of Jupiter family cometary nuclei from Deep Impact observations: The "talps" or "layered pile" model, *Icarus*, *187*, 332–344.
Bibring, J.-P., et al. (2015), 67P/Churyumov-Gerasimenko surface properties as derived from CIVA panoramic images, *Science*, *349*, doi:10.1126/science.aab0671.
Boehnhardt, H. (2004), Split comets, in *Comets II*, vol. 745, edited by M. C. Festou, H. U. Keller, and H. A. Weaver, pp. 301–316, Univ. Ariz. Press, Tucson.
Britt, D. T., D. C. Boice, B. J. Buratti, H. Campins, R. M. Nelson, J. Oberst, B. R. Sandel, S. A. Stern, L. A. Soderblom, and N. Thomas (2004), The morphology and surface processes of Comet 19/P Borrelly, *Icarus*, *167*, 45–53.
Brownlee, D. E., et al. (2004), Surface of young Jupiter family comet 81 P/Wild 2: View from the Stardust spacecraft, *Science*, *304*, 1764–1769.
Bruck-Syal, M., P. H. Schultz, J. M. Sunshine, M. F. A'Hearn, T. L. Farnham, and D. S. P. Dearborn (2013), *Icarus*, *222*, 610–624.
Capaccioni, F., et al. (2015), The organic-rich surface of comet 67P/Churyumov-Gerasimenko as seen by VIRTIS/Rosetta, *Science*, *347*, doi:10.1126/science.aaa0628.
Chen, J., and D. Jewitt (1994), On the rate at which comets split, *Icarus*, *108*, 265–271.
Cheng, A. F., N. Izenberg, C. R. Chapman, and M. T. Zuber (2002), *Meteorit. Planet. Sci.*, *37*, 1095–1105.
Colwell, J. E., A. A. S. Gulbis, M. Horányi, and S. Robertson (2005), Dust transport in photoelectron layers and the formation of dust ponds on Eros, *Icarus*, *175*, 159–169.
Crawford, D. A. (1997), Comet Shoemaker-Levy 9 fragment size estimates: How big was the parent body? in: Near-Earth objects, *Ann. N.Y. Acad. Sci.*, *822*, 155–173.
Davidsson, B. J. R., P. J. Gutiérrez, and H. Rickman (2007), Nucleus properties of comet 9P/Tempel 1 estimated from non-gravitational force modeling, *Icarus*, *187*, 306–320.

De Sanctis, M. C., et al. (2015), The diurnal cycle of water ice on comet 67P/Churyumov–Gerasimenko, *Nature*, *525*, 500–503, doi:10.1038/nature14869.
Delbo, M., G. Libourel, J. Wilkerson, N. Murdoch, P. Michel, K. T. Ramesh, C. Ganino, C. Verati, and S. Marchi (2014), Thermal fatigue as the origin of regolith on small asteroids, *Nature*, *508*, 233–236, doi:10.1038/nature13153.
Dombard, A. J., and A. M. Freed (2002), Thermally induced lineations on the asteroid Eros: Evidence of orbit transfer, *Geophys. Res. Lett.*, *29*(16), 1818, doi:10.1029/2002GL015181.
Dombard, A. J., O. S. Barnouin, L. M. Prockter, and P. C. Thomas (2010), Boulders and ponds on the Asteroid 433 Eros, *Icarus*, *210*, 713–721, doi:10.1016/j.icarus.2010.07.006.
Duxbury, T. C., R. L. Newburn, and D. E. Brownlee (2004), Comet 81P/Wild 2 size, shape, and orientation, *J. Geophys. Res.*, *109*, E12S02, doi:10.1029/2004JE002316.
El-Maarry, M. R., et al. (2015a), Fractures on comet C-G/Churyumov-Gerasimenko observed by Rosetta/OSIRIS, *Geophys. Res. Lett.*, *42*, 5170–5178, doi:10.1002/2015GL064500.
El-Maarry, M. R., et al. (2015b), Regional surface morphology of comet 67P/Churyumov-Gerasimenko from Rosetta/OSIRIS images, *Astron. Astrophys.*, *583*, A26, doi:10.1051/0004-6361/201525723.
El-Maarry, M. R., et al. (2016), Regional surface morphology of comet 67P from Rosetta/OSIRIS images: The southern hemisphere, *Astron. Astrophys.*, *593*, A110, doi:10.1051/0004-6361/201628634.
Emerich, C., et al. (1987), Temperature and size of the nucleus of Comet P/Halley deduced from IKS infrared VEGA-1 measurements, *Astron. Astrophys.*, *187*, 839–842.
Ernst, C. M., and P. H. Schultz (2007), Evolution of the Deep Impact flash: Implications for the nucleus surface based on laboratory experiments, *Icarus*, *190*, 334–344.
Farnham, T. L., and A. L. Cochran (2002), A McDonald observatory study of Comet 19P/Borrelly: Placing the Deep Space 1 observations into a broader context, *Icarus*, *160*, 398–418.
Farnham, T. L., et al. (2007), Dust coma morphology in the Deep Impact images of comet 9P/Tempel 1, *Icarus*, *187*, 26–40.
Farnham, T. L., D. Bodewits, J.-Y. Li, P. Thomas, and M. J. S. Belton (2013), Connections between the jet activity and surface features on comet 9P/Tempel 1, *Icarus*, *222*, 540–549.
Feaga, L. M., M. F. A'Hearn, J. Sunshine, O. Groussin, and T. Farnahm (2007), Asymmetries in the distribution of H_2O and CO_2 in the inner coma of comet 9P/Tempel 1 as observed by Deep Impact, *Icarus*, *190*, 345–356.
Feaga, L. M., et al. (2011), Heterogeneity of comet 103P/Hartley 2's gaseous coma, Lunar & Planetary Sci. Conf. Abstract 2461.
Fernandez, Y. R. (2009), That's the way the comet crumbles: Splitting Jupiter-family comets, *Planet. Space Sci.*, *57*, 1218–1227.
Fink, U., et al. (2016), Investigation into the disparate origin of CO_2 and H_2O outgassing for comet 67/P, *Icarus*, *277*, 78–97.
Fornasier, S., et al. (2015), Spectro-photometric properties of the 67P/Churyumov-Gerasimenko's nucleus from the OSIRIS instrument onboard the ROSETTA spacecraft, *Astron. Astrophys.*, *583*, A30, doi:10.1051/0004-6361/201525901.
Groussin, O., et al. (2013), The temperature, thermal inertia, roughness and color of the nuclei of comets 103P/Hartley 2 and 9P/Tempel 1, *Icarus*, *222*, 580–594.
Groussin, O., et al. (2015), Temporal morphological changes in the Imhotep region of comet 67P/Churyumov-Gerasimenko, *Astron. Astrophys.*, *583*, A36, doi:10.1051/0004-6361/201527020.
Grün, E., et al. (1993), Development of a dust mantle on the surface of an insolated ice-dust mixture: Results from the KOSI-9 experiment, *J. Geophys. Res.*, *98*(E8), 15,091–15,104, doi:10.1029/93JE01134.
Hartzell, C. M., X. Wang, D. J. Scheeres, and M. Horányi (2013), Experimental demonstration of the role of cohesion in electrostatic dust lofting, *Geophys. Res. Lett.*, *40*, 1038–1042, doi:10.1002/grl.50230.
Hässig, M., et al. (2015), Time variability and heterogeneity in the coma of 67P/Churyumov-Gerasimenko, *Science*, *347*, aaa0276.
Hermalyn, B., et al. (2013), The detection, localization, and dynamics of large icy particles surrounding comet 103P/Hartley 2, *Icarus*, *222*, 625–633.
Holsapple, K., and K. Housen (2007), A crater and its ejecta: An interpretation of Deep Impact, *Icarus*, *191*, 586–597.
Housen, K., and K. Holsapple (2012), Craters without ejecta, *Icarus*, *219*, 297–306.
Jansson, K. W., and A. Johansen (2014), Formation of pebble-pile planetesimals, *Astron. Astrophys.*, *570*, A47, doi:10.1051/0004-6361/201424369.
Jutzi, M., and E. Asphaug (2015), The shape and structure of cometary nuclei as a result of low-velocity accretion, *Science*, *348*, 1355–1358, doi:10.1126/science.aaa4747.
Keller, H. U., and N. Thomas (1988), On the rotation axis of Comet Halley, *Nature*, *333*, 146–148.
Keller, H. U., et al. (1986), First Halley multicolour camera imaging results from Giotto, *Nature*, *321*, 320–326.
Keller, H. U., et al. (2015), Insolation, erosion, and morphology of comet C-G/Churyumov-Gerasimenko, *Astron. Astrophys.*, *583*, A34.
Kitamura, Y., O. Ashihara, and T. Yamamoto (1985), A model for the hydrogen coma of a comet, *Icarus*, *61*, 278–295.
Kochan, H. W., W. F. Huebner, and D. W. G. Sears (1998), Simulation experiments with cometary analogous material, *Earth Moon Planets*, *80*, 369–411.
Kofman, W., et al. (2015), Properties of the interior of the nucleus of 67P/Churyumov- Gerasimenko revealed by CONSERT radar, *Science*, *349*, doi:10.1126/science.aab0639.
Kossacki, K. J., N. I. Kömle, J. Leliwa-Kopystynski, and G. Kargl (1997), Laboratory investigation of the evolution of cometary analogs: Results and interpretation, *Icarus*, *128*, 127–144.
Kührt, E. (1984), Temperature profiles and thermal stresses in cometary nuclei, *Icarus*, *60*, 512–521.
Kührt, E., and H. U. Keller (1994), The formation of cometary surface crusts, *Icarus*, *109*, 121–132.
Lethuillier, A., A. Le Gall, M. Hamelin, W. Schmidt, K. J. Seidensticker, R. Grard, V. Ciarletti, S. Caujolle-Bert, H.-H. Fischer, and R. Trautner (2016), Electrical properties and porosity of the first meter of the nucleus of 67P/Churyumov-Gerasimenko. As constrained by the Permittivity Probe SESAME-PP/Philae/Rosetta, *Astron. Astrophys.*, *591*, A32, doi:10.1051/0004-6361/201628304.
Levy, J. S., D. R. Marchant, and J. W. Head (2010), Thermal contraction crack polygons on Mars: A synthesis from HiRISE, Phoenix, and terrestrial analog studies, *Icarus*, *206*(1), 229–252, doi:10.1016/j.icarus.2009.09.005.
Li, J.-Y., et al. (2007), Deep Impact photometry of comet 9P/Tempel 1, *Icarus*, *187*, 41–55.
Li, J.-Y., et al. (2013), Photometric properties of the nucleus of comet 103P/Hartley 2, *Icarus*, *222*, 559–570.
Möhlmann, D. (1994), Surface regolith and environment of comets, *Planet. Space Sci.*, *42*, 933–937.
Molaro, J. L., S. Byrne, and S. A. Langer (2015), Grain-scale thermoelastic stresses and spatiotemporal temperature gradients on airless bodies, implications for rock breakdown, *J. Geophys. Res. Planets*, *120*, 255–277, doi:10.1002/2014JE004729.
Mottola, S., et al. (2015), The structure of the regolith on 67P/Churyumov-Gerasimenko from ROLIS descent imaging, *Science*, *349*, doi:10.1126/science.aab0232.

Mousis, O., et al. (2015), Pits formation from volatile outgassing on 67P/Churyumov-Gerasimenko, *Astrophys. J. Lett.*, *814*, L5.
Mumma, M. J., and S. B. Charnley (2011), The chemical composition of comets—Emerging taxonomies and natal heritage, *Ann. Rev. Astron. Astrophys.*, *49*, 471–524.
O'Brien, D. P., R. Greenberg, and J. E. Richardson (2006), Craters on asteroids: Reconciling diverse impact records with a common impacting population, *Icarus*, *183*, 79–92.
Pähtz, T., and O. Durán (2016), Transport-threshold model suggests sand transport by wind on Triton, Pluto, and 67P/C-G, *Atmos. Oceanic Phys.*arXiv:1602.07079.
Pajola, M., et al. (2015), Size-frequency distribution of boulders ≥7 m on comet 67P/Churyumov-Gerasimenko, *Astron. Astrophys.*, *583*, A37.
Pätzold, M., et al. (2016), A homogeneous nucleus for comet 67P/Churyumov-Gerasimenko from its gravity field, *Nature*, *530*, 63–65.
Poch, O., A. Pommerol, B. Jost, N. Carrasco, C. Szopa, and N. Thomas (2016), Sublimation of ice-tholins mixtures: A morphological and spectrophotometric study, *Icarus*, *266*, 288–305.
Pommerol, A., et al. (2015), OSIRIS observations of metre-size exposures of H_2O ice at the surface of 67P/Churyumov-Gerasimenko and interpretation using laboratory experiments, *Astron. Astrophys.*, *583*, A25, doi:10.1051/0004-6361/201525977.
Poppe, A. R., J. S. Halekas, G. T. Delory, W. M. Farrell, V. Angelopoulos, J. P. McFadden, J. W. Bonnell, and R. E. Ergun (2012), A comparison of ARTEMIS observations and particle-in-cell modeling of the lunar photoelectron sheath in the terrestrial magnetotail, *Geophys. Res. Lett.*, *39*, L01102, doi:10.1029/2011GL050321.
Prialnik, D. (1997), A model for the distant activity of comet Hale-Bopp, *Astrophys. J.*, *478*, L107–L110.
Richardson, J. E., H. J. Melosh, C. M. Lisse, and B. Carcich (2007), A ballistics analysis of the Deep Impact ejecta plume: Determining comet Tempel-1's gravity, mass, and density, *Icarus*, *190*, 357–390.
Roberts, J. H., E. G. Kahn, O. S. Barnouin, C. M. Ernst, L. M. Prockter, and R. W. Gaskell (2014), Origin and flatness of ponds on asteroid 433 Eros, *Meteorit. Planet. Sci.*, *49*, 1735–1748.
Robinson, M. S., P. C. Thomas, J. Veverka, S. Murchie, and B. Carcich (2001), The nature of ponded deposits on Eros, *Nature*, *413*, 396–400.
Rotundi, A., et al. (2015), Dust measurements in the coma of comet C-G/Churyumov-Gerasimenko inbound to the Sun, *Science*, *347*, aaa3905.
Rubin, M., N. Fougere, K. Altwegg, M. R. Combi, L. Le Roy, V. M. Tenishev, and N. Thomas (2014), Mass transport around comets and its impact on the seasonal differences in water production rates, *Astrophys. J.*, *788*, 168.
Sagdeev, R. Z., et al. (1986), TV experiment in Vega mission: Image processing technique and some results, in *20th ESLAB Symposium on the Exploration of Halley's Comet*, vol. 2, edited by B. Battrick et al., pp. 295–305 , ESA SP-250, Noordwijk, Netherlands.
Sears, D. W. G., L. L. Tornabene, G. R. Osinski, S. S. Hughes, and J. L. Heldmann (2015), Formation of the "ponds" on asteroid (433) Eros by fluidization, *Planet. Space Sci.*, *117*, 106–118.
Sekanina, Z. (1991), Cometary activity, discrete outgassing areas, and dust-jet formation, in *IAU Colloquium No. 116: Comets in the Post-Halley Era*, *Astrophysics and Space Science Library*, vol. 167, edited by R. L. Newburn Jr., M. Neugebauer, and J. Rahe, pp. 769–823, Kluwer Acad., Dordrecht, Netherlands.
Schroeder, S., et al. (2016), *The ROLIS post-landing images of comet Churyumov-Gerasimenko*, p. 8288, EGU General Assembly, Vienna.
Schultz, P.H., C. A. Eberhardy, C. M Ernst, M. F. A. A'Hearn, J. M. Sunshine, C. M. Lisse (2007), The DI oblique cratering experiment, *Icarus*, *190*, 295–333.
Sierks, H., et al. (2015), On the nucleus structure and activity of comet C-G/Churyumov-Gerasimenko, *Science*, *347*, doi:10.1126/science.aaa1044.
Soderblom, L. A., et al. (2002), Observations of comet 19P/Borrelly by the miniature integrated camera and spectrometer aboard Deep Space 1, *Science*, *296*, 1087–1091.
Soderblom, L. A., D. T. Britt, R. H. Brown, B. J. Buratti, R. L. Kirk, T. C. Owen, and R. V. Yelle (2004), Short-wavelength infrared (1.3–2.6 μm) observations of the nucleus of comet 19P/Borrelly, *Icarus*, *167*, 100–112.
Spohn, T., et al. (2015), Thermal and mechanical properties of the near-surface layers of comet 67P/Churyumov-Gerasimenko, *Science*, *349*, doi:10.1126/science.aab0464.
Sunshine, J. M., et al. (2007a), Exposed water ice deposits on the surface of comet 9P/Tempel 1, *Science*, *311*, 1453–1455.
Sunshine, J. M., O. Groussin, P. H. Schultz, M. F. A'Hearn, L. M. Feaga, T. L. Farnham, and K. P. Klaasen (2007b), The distribution of water ice in the interior of comet Tempel 1, *Icarus*, *190*, 284–294.
Sunshine, J. M., et al. (2011), Icy Grains in Comet 103P/Hartley 2, 42nd Lunar and Planetary Science Conference, Abstract 2292.
Tauber, F., and E. Kührt (1987), Thermal stresses in cometary nuclei, *Icarus*, *69*, 83–90.
Thomas, N., C. Alexander, and H. U. Keller (2008), Loss of the surface layers of comet nuclei, *Space Sci. Rev.*, *138*, 165–177.
Thomas, N., et al. (2015a), The morphological diversity of comet C-G/Churyumov-Gerasimenko, *Science*, *347*, doi:10.1126/science.aaa0440.
Thomas, N., et al. (2015b), Redistribution of particles across the nucleus of comet C-G/Churyumov-Gerasimenko, *Astron. Astrophys.*, *583*, A17.
Thomas, P. C., et al. (2007), The shape, topography, and geology of Tempel 1 from Deep Impact observations, *Icarus*, *187*, 4–15.
Thomas, P. C., et al. (2013a), The nucleus of comet 9P/Tempel 1: Shape and geology from two flybys, *Icarus*, *222*, 453–466.
Thomas, P. C., et al. (2013b), Shape, density, and geology of the nucleus of comet 103P/Hartley 2, *Icarus*, *222*, 550–558.
Veverka, J., et al. (2013), Return to comet Tempel 1: Overview of Stardust NExT results, *Icarus*, *222*, 424–435.
Vincent, J.-B., et al. (2015), Large heterogeneities in comet C-G as revealed by active pits from sinkhole collapse, *Nature*, *523*, 63–66.
Vincent, J.-B., et al. (2016), Are fractured cliffs the source of cometary dust jets? Insights from OSIRIS/Rosetta at C-G/Churyumov-Gerasimenko, *Astron. Astrophys.*, *587*, A14.